ASCE

Experimental Study on Early-Age Cracking Behavior of Hooked-End Steel Fiber–Reinforced Concrete under Different Curing Temperatures

Jiacheng Kang[1]; Dejian Shen[2]; Haoze Shao[3]; Quan Huang[4]; and Xingzuo Liu[5]

Abstract: Steel fiber is the most widely used type of fiber in concrete because of its advanced and economical manufacturing facilities, reinforcing effect, and ability to cope with changing environmental conditions. The use of steel fiber in concrete can reduce the amount of reinforcement used and increase the crack resistance of concrete, which extends the service life of concrete structures, reduces the frequency of maintenance and repairs, and consequently lowers energy consumption and emissions. Many studies focus on the postcracking behavior of steel fiber–reinforced concrete (SFRC). However, it is also crucial to examine the precracking behavior of SFRC at early age. A temperature stress test machine (TSTM) was used to investigate the autogenous shrinkage (AS), tensile creep (TC), and cracking behavior of hooked-end SFRC (HSFRC) at early age under uniaxial constant restrained condition. Analysis and experimental findings demonstrated that (1) the addition of steel fiber increased the splitting tensile strength and modulus of elasticity of HSFRC. The 1-, 3-, and 7-day splitting tensile strength and modulus of elasticity increased with an increase in curing temperature. However, a decrease was observed at 28 days as the curing temperature increased; (2) increasing steel fiber content had a significant influence on reducing TC and AS of HSFRC. TC and AS of HSFRC increased with increasing curing temperature; and (3) early-age cracking potential of HSFRC decreased as steel fiber content increased. Increased curing temperature resulted in a concomitant elevation in the potential for early-age cracking in HSFRC. **DOI: 10.1061/JMCEE7.MTENG-17246.**

Author keywords: Steel fiber–reinforced concrete; Curing temperature; Cracking potential; Tensile creep; Autogenous shrinkage.

Introduction

Nowadays, the utilization of concrete composites reinforced with advanced fibers, including basalt fibers (Li et al. 2022), glass fibers (Guzlena and Sakale 2021), carbon fibers (Liu et al. 2020), polymer fibers (Chen et al. 2020), and steel fibers (Abdallah et al. 2016) has become prevalent within the construction industry. Steel fiber is the most widely used one among various kinds of fibers and is considered an adequate choice for concrete because of its advanced and economical manufacturing facilities, reinforcing effect, and ability to cope with changing environmental conditions (Afroughsabet et al. 2016; Kalpana and Tayu 2020). The use of steel fiber in concrete reduces the amount of reinforcement used, leading to a decrease in the consumption of building materials and reliance on natural resources. Moreover, the addition of steel fibers enhances the crack resistance of concrete, resulting in an extended service life for concrete structures, reduced maintenance and repair frequency, and lowered energy consumption and emissions (Shao et al. 2022; Wang et al. 2023). Steel fiber–reinforced concrete (SFRC) is applied in various concrete constructions, such as maritime applications and tunnel linings (Da Silva et al. 2020). Steel fibers are randomly distributed throughout the concrete, which transfers the internal stress before cracks appear. When cracking occurs in the concrete matrix, steel fibers play a crucial role as crack-bridging agents, effectively retarding crack propagation (Afroughsabet et al. 2016). The addition of steel fibers transforms the material from a brittle to a pseudo-ductile behavior (Haddad and Smadi 2004). Steel fiber can be categorized into different geometric shapes, such as straight, crimped, spiral, twisted, and hooked-end steel fibers (Abdallah et al. 2017). Hooked-end steel fiber, known for its high mechanical anchorage effect and high tensile strength, is the most wide type in the market (Da Silva et al. 2020). Numerous studies have been conducted on various properties of SFRC, including mechanical properties (Alrawashdeh and Eren 2022), fracture properties (Murugan et al. 2020), durability properties (Afroughsabet et al. 2016), and pull-out strength (Abdallah et al. 2018). In general, the addition of steel fibers to concrete enhances its mechanical properties (Afroughsabet et al. 2016). Concrete subjected to restraint because of its limited tensile strength and strain capacity may develop cracks over time (Bentz and Snyder 1999), allowing moisture and aggressive chemical ions, such as bromine and acid sulfate, to penetrate and compromise its quality (Hubert et al. 2014). The formation of cracks at early age can negatively affect

[1]Research Student, College of Civil and Transportation Engineering, Hohai Univ., No. 1, Xikang Rd., Nanjing 210098, China. Email: kangjiachenghhu@hhu.edu.cn

[2]Professor, College of Civil and Transportation Engineering, Hohai Univ., No. 1, Xikang Rd., Nanjing 210098, China; Jiangsu Engineering Research Center for Crack Control in Concrete, No. 1, Xikang Rd., Nanjing 210098, China; Nanjing Engineering Research Center for Prefabricated Construction, No. 1, Xikang Rd., Nanjing 210098, China (corresponding author). ORCID: https://orcid.org/0000-0002-0283-6835. Email: shendjn@163.com

[3]Research Student, College of Civil and Transportation Engineering, Hohai Univ., No. 1, Xikang Rd., Nanjing 210098, China. Email: hzshao@hhu.edu.cn

[4]Research Student, College of Civil and Transportation Engineering, Hohai Univ., No. 1, Xikang Rd., Nanjing 210098, China. Email: qhuang@hhu.edu.cn

[5]Research Student, College of Civil and Transportation Engineering, Hohai Univ., No. 1, Xikang Rd., Nanjing 210098, China. Email: liuxingzuohhu@163.com

Note. This manuscript was submitted on July 2, 2023; approved on February 22, 2024; published online on July 16, 2024. Discussion period open until December 16, 2024; separate discussions must be submitted for individual papers. This paper is part of the ***Journal of Materials in Civil Engineering***, © ASCE, ISSN 0899-1561.

the concrete quality and compromise the structural integrity of buildings (Sahmaran et al. 2015). Therefore, numerous investigations have been conducted to examine the cracking characteristics of SFRC (Barros et al. 2005; Frazão et al. 2022). However, most studies in the field of SFRC focus on postcracking behavior, considering the primary function of steel fibers in bridging cracks and transferring stress across them once initial cracking occurs. It is equally crucial to examine the precracking behavior of SFRC at early age (Afroughsabet et al. 2016). Hence, investigations on the early-age cracking behavior of hooked-end SFRC (HSFRC) are necessary.

Early-age cracking behavior is affected by complex interactions of mechanical properties, tensile creep (TC), thermal, and autogenous shrinkage (AS) (Mehta and Monteiro 2014; Wei et al. 2017). TC plays a significant role in early-age concrete among these factors, and it is essential in decreasing shrinkage-induced stress. Many investigations have been published on the creep of concrete reinforced with fibers (Garas et al. 2009; Zheng et al. 2019), while unclear conclusions about the influence of fiber on the TC are drawn because of significant variations in experimental data. Zheng et al. (2019) studied the TC of lightweight aggregate SFRC with different steel fiber contents (0, 0.5%, 1%, and 2%). The results showed that the TC was reduced significantly by adding steel fiber. Garas et al. (2009) also reported similar results on TC in the research on ultrahigh-performance concrete (UHPC) reinforced by steel fiber. However, Bissonnette and Pigeon (1995) reported an opposing trend, indicating that TC increased by adding steel fibers. These studies reveal that variations in the contents of steel fibers incorporated into concrete have a varied impact on its TC, and that the influence of steel fibers on TC also differs with the shape of the fibers. Therefore, the study of the effect of hooked-end steel fibers on the TC of SFRC is necessary. The existing studies reveal that the curing temperature significantly impacts the creep of concrete (Jin et al. 2021; Wei et al. 2017; Zhao et al. 2015). However, the conclusions drawn from previous studies on TC of concrete cured at different temperatures are controversial. Wei et al. (2017) studied early-age TC of concrete cured at 23°C and 43°C. The results revealed that an increase in curing temperature promoted the development of TC. A similar finding was also reported by Hauggaard et al. (1999). However, the TC of steel fiber–reinforced UHPC was investigated in the study by Garas et al. (2012), which depicted that TC of UHPC cured at 90°C for 48 h decreased by about 63% when compared to the UHPC without thermal treatment. This reduction can be chiefly attributed to the accelerated cement hydration at a high temperature leading to an early strength gain and a denser microstructure, which in turn potentially reduces TC. Further investigations are necessary to evaluate the effects of curing temperature and steel fiber content on the TC of HSFRC at early age. The accuracy of creep measurement of early-age concrete would be affected by the development of AS (Lee et al. 2006). Thus, AS of early-age HSFRC at different curing temperatures is of great importance to be investigated to more accurately assess the TC and cracking behavior of SFRC at early age.

A temperature stress test machine (TSTM) is designed to examine the characteristics of concrete, such as temperature process, restrained stress, AS, and TC behavior of concrete under uniaxial constant restrained conditions. Springenschmid et al. (1968) developed the first TSTM to investigate the restrained stress caused by hydration heat in 1985. In 1994, Kovler proposed a closed-loop restraining system for a TSTM based on the principles proposed by Bloom and Bentur (1993). A TSTM could control the temperature process of concrete by utilizing the temperature-controlling molds and create an adiabatic environment to more accurately simulate the working conditions of mass concrete under uniaxial constant restrained condition. In addition, the TC values measured in the TSTM test (uniaxial constant restrained condition) are different from those obtained from the direct tensile test because of different restraint degrees. The TC values obtained from these two conditions might even result in opposing conclusions (Kolver et al. 1999; Shen et al. 2020; Zhang and Qin 2006). A TSTM was used to investigate the TC and AS of concrete reinforced with 5D hooked-end steel fiber volume fraction (0, 0.12%, 0.24%, and 0.36%) by Kang et al. (2023). However, the effects of different steel fiber shapes, higher steel fiber contents, and different curing temperatures on TC and AS of HSFRC were not clear. Most importantly, at this stage, there are no studies that simultaneously consider the effects of curing temperature and steel fiber content on the early-age cracking potential in hooked-end steel fiber–reinforced concrete under the combined influences of temperature, shrinkage, creep, and restrained stress. Therefore, utilizing a TSTM to investigate the effects of steel fiber content and curing temperature on early-age cracking behavior of HSFRC under uniaxial constant restrained condition is necessary.

This research aimed to investigate the effects of steel fiber content and curing temperature on early-age AS, TC, and cracking behavior of HSFRC under uniaxial constant restrained condition To achieve this, effects of different steel fiber contents (0, 0.3%, 0.6%, and 0.9% by volume of concrete) and curing temperatures (20°C, 35°C, and 50°C) on temperature, restrained stress, AS, and TC of HSFRC at early age were evaluated with TSTM.

Experimental Program

Mixture Proportions and Materials

In this research, six mixtures with a water-to-cement (w/c) ratio of 0.37 were prepared. Mixtures SF06-20, SF06-35, and SF06-50 were subjected to three curing temperatures (20°C, 35°C, and 50°C), respectively, with a constant steel fiber content of 0.6%. Additionally, Mixtures SF00-20, SF03-20, SF06-20, and SF09-20 were subjected to the curing temperature of 20°C, with varying steel fiber contents of 0, 0.3%, 0.6%, and 0.9%, respectively. Hooked-end steel fibers (Dramix 3D steel fibers manufactured by Bekaert) were utilized to substitute coarse aggregates partly by volume, as recommended by Nataraja et al. (1999). Table 1 depicts the compositions and curing temperatures of six mixtures. The same raw materials were utilized in six mixtures.

Ordinary portland cement (PO 42.5) was utilized in accordance with Chinese National Standard GB 175 (Chinese Standard 2018) and ASTM C150 (ASTM 2020). Table 2 presents the chemical and physical properties of ordinary portland cement. The coarse aggregate was crushed limestone with particle sizes ranging from 5 to 25 mm, and the fine aggregate was natural river sand with a fineness modulus of 2.25. The hooked-end steel fiber used in this research had a length of 60 mm and a diameter of 0.75 mm, as depicted in Fig. 1. The hook length and angle of the steel fiber were about 4 mm and 45°, respectively. A polycarboxylate-based superplasticizer was employed to regulate the workability of the mixture. The slump values obtained for Mixtures SF00-20, SF03-20, SF06-20, SF09-20, SF06-35, and SF06-50 were 165, 153, 142, 131, 142, and 142 mm, respectively.

During specimen preparation, the mixer was utilized to blend dry components, including coarse aggregates, fine aggregates, cement, and steel fibers, for 3 min to ensure consistent distribution of ingredients. Tap water was added into the mixer gradually, along with the superplasticizer. The resultant mixture was mixed for 3 min to complete the process.

Table 1. Mixture proportions and curing temperatures of HSFRC

Mixture composition	Unit	SF00-20	SF03-20	SF06-20	SF09-20	SF06-35	SF06-50
Water	kg/m^3	170	170	170	170	170	170
Cement	kg/m^3	456	456	456	456	456	456
Fine aggregate	kg/m^3	710	710	710	710	710	710
Coarse aggregate	kg/m^3	1,064.0	1,055.9	1,047.8	1,039.7	1,047.8	1,047.8
Superplasticizer	kg/m^3	4.05	4.05	4.05	4.05	4.05	4.05
Hooked-end steel fiber	kg/m^3	0	23.55	47.10	70.65	47.10	47.10
Steel fiber content	%	0	0.3	0.6	0.9	0.6	0.6
Curing temperature	°C	20	20	20	20	35	50

Table 2. Chemical and physical properties of ordinary portland cement

Item	Value
SiO_2	19.9%
Al_2O_3	4.6%
Fe_2O_3	3.0%
CaO	64.6%
MgO	0.78%
SO_3	2.37%
Na_2O	0.06%
K_2O	0.65%
Cl–	0.01%
3-day compressive strength	21.8 MPa
28-day compressive strength	47.6 MPa
Blaine fineness	342 m^2/kg
Initial setting time	182 min
Final setting time	251 min

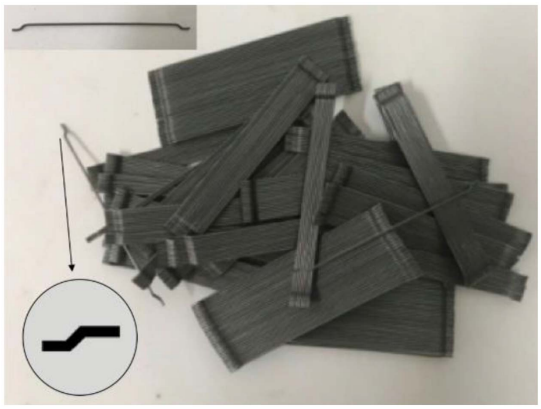

Fig. 1. Hooked-end steel fiber.

Mechanical Test

The splitting tensile strength and modulus of elasticity of six mixtures at different ages were tested in accordance with the Chinese Standard GB/T 50081 (Chinese Standard 2019). The splitting tensile strength was tested on concrete cubes with a dimension of 150 × 150 × 150 mm; the modulus of elasticity was tested on concrete prims with a dimension of 150 × 150 × 300 mm. After being poured, the samples were covered with plastic film and were removed from molds after 1 day. Subsequently, samples of Mixtures SF00-20, SF03-20, SF06-20, and SF09-20 were subjected to curing at a constant temperature of 20°C in a temperature- and humidity-controlled curing cabinet until the moment of testing. Samples of the mixtures labeled SF06-35 and SF06-50 were placed in a curing cabinet, where they were cured at constant temperatures of 35°C and 50°C, respectively, until the time of testing. The relative humidity in the cabinet was over 95%. The final results for splitting tensile strength and modulus of elasticity were the average of the results of three identical samples. The 28-day compressive strength tested for Mixtures SF00-20, SF03-20, SF06-20, SF09-20, SF06-35, and SF06-50 were 40.60, 45.05, 47.35, 49.72, 48.12, and 50.32 MPa, respectively.

TSTM Test

Testing Equipment

Fig. 2 depicts that TSTM comprises two dog bone–shaped molds, a stepper motor, a temperature control system, a displacement measurement system, and a load recording system. The primary structure of the TSTM consists of two horizontal steel frames, with stainless steel supports located beneath the horizontal frame. Two molds of identical dimensions were used for the measurement of free and restrained shrinkage deformations. The interior of the TSTM mold is composed of an aluminum alloy template, while the exterior consists of an insulating layer. The insulating layer is constructed with wooden boards on the exterior and insulating foam on the interior. Numerous water pipes are arranged within the blue insulating layer for circulating liquid, allowing for the control of concrete specimen temperature by adjusting the temperature of the circulating liquid. The length of the center part of the molds was 1,500 mm. The deformation was measured using a displacement sensor that was installed on the straight section of the specimens. The gripped end of the restrained shrinkage specimen was attached to a stepper motor. In this research, when the incremental deformation of the restrained specimen approached 2 μm, the stepper motor was used to pull or push the restrained shrinkage specimen back to the original position, thus ensuring it was subjected to full restraint (Zhang and Qin 2006). The temperature and the restrained stress of specimens were monitored utilizing the temperature sensor and load cell, respectively. The heating–cooling system in the TSTM was utilized to regulate the temperature process of concrete. In the TSTM test, a restrained specimen and a free specimen were tested for one mixture.

Testing Procedure and Curing Mode

As recommended by Wei and Hansen (2013), the mold was covered with a plastic film sheet to minimize friction between the molds and the concrete specimens prior to fresh concrete being poured directly into the molds, then each concrete specimen was promptly sealed to diminish moisture evaporation. Concrete specimens were subjected to the same curing mode in a single test, as recommended by Shen et al. (2016). Data collection using a computer started immediately following the pouring process, and the data were recorded at an interval of 5 min.

The TSTM tests were conducted at temperature-controlled conditions using a constant-temperature curing mode. The effect of

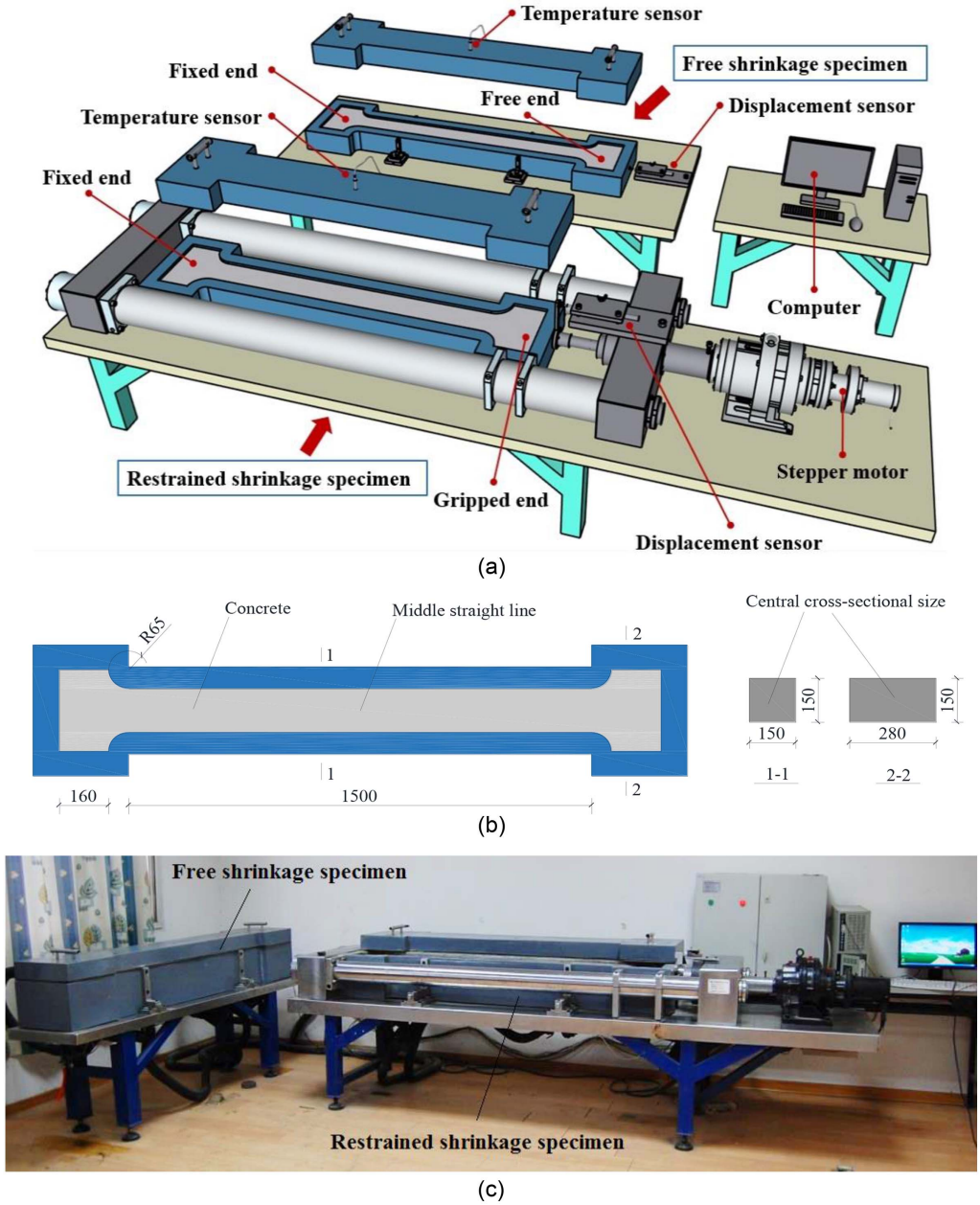

Fig. 2. (a) Schematic diagram of TSTM; (b) schematic diagram of specimen mold (mm); and (c) photo of TSTM.

curing temperature on the properties of HSFRC at early age was studied. Three curing temperatures (20°C, 35°C, and 50°C) were used in this research. Mixtures SF00-20, SF03-20, SF06-20, and SF09-20 were subjected to a constant temperature of 20°C for 240 h after pouring. To ensure that the maturity of Mixtures SF06-35 and SF06-50 was similar to that of Mixture SF06-20 when the temperature of Mixtures SF06-35 and SF06-50 reached 20°C, Mixtures SF06-35, and SF06-50 were cured at constant temperatures of 35°C and 50°C for 112 and 50 h, respectively. Eq. (1) was used to determine the duration of curing at peak temperature, as recommended by Shen et al. (2016)

$$t_e = \int_0^t \exp\left[\frac{E_a(T)}{R}\left(\frac{1}{T_{ref}+273}-\frac{1}{T(t)+273}\right)\right]dt \quad (1)$$

where t_e = equivalent age of 20°C; t = age of concrete (in days); $E_a(T)$ = activation energy (in kJ/mol); R = ideal gas constant (8.315 J · mol^{-1} · K^{-1}); T_{ref} = reference temperature of 20°C; and $T(t)$ = time-dependent temperature (in °C).

Subsequently, the temperature of the concrete specimen was gradually decreased at a rate of 1°C/h until cracking. To reduce the impact of viscoelastic and thermal gradients, the rate of 1.0°C/h was employed in this research, as recommended by Shen et al. (2016). The temperature process of constant-temperature curing mode for the TSTM test is depicted in Fig. 3.

Calculation Procedure of AS

The deformation of concrete measured in a closed system is referred to as AS, which is sometimes known as self-desiccation shrinkage. This measurement excludes volume changes due to the loss or ingress of substances, variations in temperature, and the application of external force and restraint. In all types of concrete, some degree of AS is observed; however, it is particularly significant in high-strength concrete, characterized by high cement

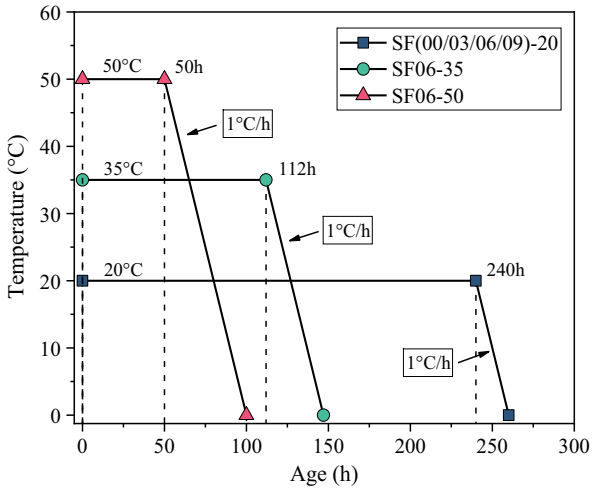

Fig. 3. Temperature process of constant temperature curing mode for TSTM test.

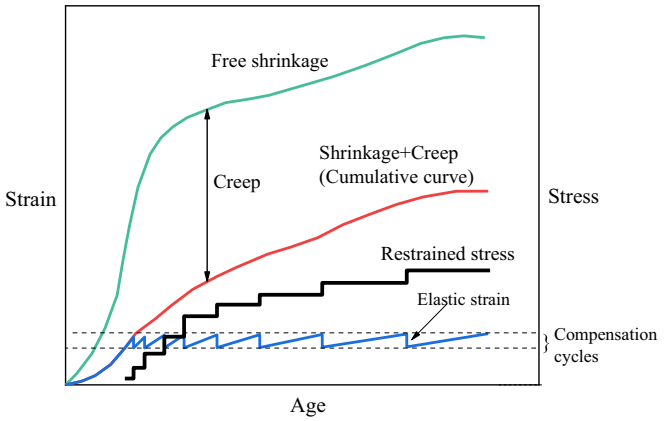

Fig. 4. Correlation between elastic strain, creep, and free shrinkage. (Reprinted from K. Kovler et al., "Tensile creep behavior of high strength concretes at early ages," *Materials and Structures*, Vol. 32, pp. 383–387, © 1999, Springer Nature.)

content and a low water-to-cement ratio, where it cannot be ignored (Mehta and Monteiro 2014).

AS can be determined by computing the difference between the total deformation and thermal deformation, as given in Eq. (2) (Chu et al. 2012)

$$\varepsilon_{as} = \varepsilon_{tf} - \alpha \times \Delta T \tag{2}$$

where ε_{as} = AS deformation (in $\mu\varepsilon$); ε_{tf} = total deformation of free shrinkage specimen (in $\mu\varepsilon$); α = coefficient of thermal expansion (CTE) (in $\mu\varepsilon$/°C); and ΔT = temperature change (in °C).

Given that the CTE value can change over time and with variations in moisture content in concrete (Sellevold and Bjøntegaard 2006), a modified prediction model was employed to determine the CTE value, as given in Eq. (3) (Shen et al. 2017)

$$\alpha_T(t) = \alpha_k \times [1 + 41 \times (t \cdot 24)^{-m}] \tag{3}$$

where $\alpha_T(t)$ = CTE value that changes over time (in $\mu\varepsilon$/°C); α_k = mean value of CTE during cooling period (in $\mu\varepsilon$/°C); and $m = 2.0$.

Eq. (4) was employed to determine the mean value of CTE during the cooling period, considering that the results of CTE tend to stabilize after 24 h when concrete is cured at 20°C (Viviani et al. 2007)

$$\alpha_k = \frac{\Delta\varepsilon}{\Delta T} = \frac{\varepsilon_{ckf} - \varepsilon_{cof0}}{T_{ckf} - T_{cof0}} \tag{4}$$

where ε_{ckf} = strain of free shrinkage specimen at cracking age (in $\mu\varepsilon$); ε_{cof0} = strain of free shrinkage specimen at the initiation of the cooling period (in $\mu\varepsilon$); T_{ckf} = temperature of free shrinkage specimen at cracking age (in °C); and T_{cof0} = temperature of free shrinkage specimen at the initiation of the cooling period (in °C). The results of the mean value of CTE during the cooling period for Mixtures SF00-20, SF03-20, SF06-20, SF09-20, SF06-35, and SF06-50 were 7.80, 7.79, 6.51, 5.98, 6.56, and 6.51 $\mu\varepsilon$/°C, respectively.

Eq. (5) was employed to determine AS in this research, as recommended by Chu et al. (2012)

$$\varepsilon_{as}(t) = \varepsilon_{tf}(t) - \alpha_T(t) \times [T(t) - T_{time-zero}] \tag{5}$$

where $\varepsilon_{as}(t)$ = AS that changes over time (in $\mu\varepsilon$); and $T_{time-zero}$ = time-zero temperature (in °C). Given that the rigidity of fresh concrete is low and no stress was produced during the TSTM test, the value of AS is established to be zero prior to the time-zero point (Bentur 2001; Lura et al. 2001). The methods for determining the time-zero point are different (Bentur 2001; Darquennes et al. 2011; Huang and Ye 2017; Lura et al. 2001; Meddah and Tagnit-Hamou 2011). Given that this research focused on the examination of deformation caused by stress, the point at which the restrained stress occurred was established as the time-zero point of deformation (Cusson and Hoogeveen 2007; Lura et al. 2001).

Calculation Procedure of TC

The calculation of early-age concrete creep through the TSTM test is given in Eq. (6), as recommended by Kovler (1994)

$$\varepsilon_{tr} = \varepsilon_{sh} + \varepsilon_c + \varepsilon_e = 0 \tag{6}$$

where ε_{tr} = total strain of restrained shrinkage specimen (in $\mu\varepsilon$); ε_{sh} = free shrinkage (in $\mu\varepsilon$); ε_c = creep (in $\mu\varepsilon$); and ε_e = elastic strain (in $\mu\varepsilon$). The ε_c and ε_e were positive values, the deformation directions of which were the same as the tensile stress, and the ε_{sh} was a negative value. Fig. 4 depicts the correlation between elastic strain, creep, and free shrinkage. In the TSTM test, free shrinkage is obtained from the free shrinkage specimen. However, the restrained specimen, besides exhibiting shrinkage deformation, experiences creep under the external constraint loads, owing to being repeatedly pulled and compressed back to its original position during the compensation cycles. The elastic strain of the restrained specimen during each cycle is recorded, thereby cumulatively calculating the total deformation of the restrained specimen. Since the only varying factor between the free and restrained specimens is the restraint condition, with all other factors held constant, the difference in deformation between the two specimens can be utilized to determine the magnitude of creep. In this research, only basic creep was considered, as the specimens were maintained in a sealed condition during the TSTM test.

Specific TC is commonly expressed as basic TC per unit of applied stress when the loading is maintained at a constant level (Kolver et al. 1999; Mehta and Monteiro 2014). In this research, given that the restrained stress changed over time, specific TC was expressed as the ratio of cumulative basic TC to the corresponding restrained stress, as recommended by Zhao et al. (2019). Eq. (7) was employed to determine the specific creep (Cusson and Hoogeveen 2007)

$$C_{sp}(t) = \frac{\Delta\varepsilon_c(t)}{\sigma_c(t)} \tag{7}$$

where $C_{sp}(t)$ = specific creep at t h (in $\mu\varepsilon$/MPa); $\Delta\varepsilon_c(t)$ = cumulative basic TC at t h (in $\mu\varepsilon$); and $\sigma_c(t)$ = restrained stress at t h (in MPa).

The creep–shrinkage ratio calculated utilizing Eq. (8) plays a crucial role in assessing the early-age relaxation behavior of concrete (Zhang and Qin 2006)

$$K(t) = \frac{\Delta\varepsilon_c(t)}{\varepsilon_{sh}(t)} \tag{8}$$

where $K(t)$ = creep–shrinkage ratio at t h; and $\varepsilon_{sh}(t)$ = free shrinkage at t h (in $\mu\varepsilon$).

Calculation Procedure of Stress Reserve

The cracking potential could be evaluated utilizing stress reserve, as given in Eq. (9) (Shen et al. 2016; Shi et al. 2014)

$$\varphi = \frac{(\sigma_{cr} - \sigma_{rt})}{\sigma_{cr}} \times 100\% \tag{9}$$

where φ = stress reserve; σ_{cr} = cracking stress (in MPa); and σ_{rt} = stress at room temperature (in MPa).

Results and Discussion

Mechanical Properties of HSFRC

Splitting Tensile Strength

Fig. 5(a) depicts the test results splitting tensile strength at 1, 3, 7, and 28 day, which are expressed as the mean values of three identical specimens. The splitting tensile strength of all concrete mixtures increased with age because of the continued formation of calcium silicate hydrate (C-S-H) during the ongoing hydration process of cement. At a consistent curing temperature of 20°C, there was generally an enhancement in the splitting tensile strength as the steel fiber contents increased at all ages. Steel fibers act as dispersed reinforcements, forming a three-dimensional network that resists crack propagation by bridging across cracks. The crack-bridging effect prevents the development and propagation of cracks, ultimately increasing the tensile capacity of concrete. Additionally, steel fibers help disperse and distribute stresses, reducing stress concentrations and enhancing the concrete's ability to withstand tension. The inclusion of steel fibers provides localized reinforcement, similar to traditional steel reinforcement, further improving the material's resistance to tensile forces (Afroughsabet et al. 2016). For instance, the 28-day splitting tensile strength for Mixtures SF00-20, SF03-20, SF06-20, and SF09-20 was 2.88, 3.12, 3.29, and 3.68 MPa, which increased by 8.3%, 14.2%, and 27.8% as steel fiber content increased from 0 to 0.3%, 0.6%, and 0.9%, respectively. A similar trend can be found in other studies concerning the splitting tensile strength of concrete reinforced with various contents of steel fibers (Mohammadi et al. 2008; Sahmaran and Yaman 2007; Yazici et al. 2007). Fig. 6 depicts the increased degree of splitting tensile strength with increasing contents of steel fibers in different shapes in Mohammadi et al. (2008), Sahmaran and Yaman (2007), and Yazici et al. (2007). To minimize the impact of the concrete matrix on the experimental results, the percentage increase of splitting tensile strength with the addition of different shapes and contents of steel fibers was calculated based on the results of the respective reference groups without steel fibers. The results reveal that, within a specific range of fiber volume fraction, the enhancement in tensile strength exhibits an approximately linear correlation. Among the assessed fiber types, hooked-end steel fibers demonstrated the most pronounced enhancements in tensile strength across varying volume fractions, while straight steel fibers yielded relatively minimal enhancements.

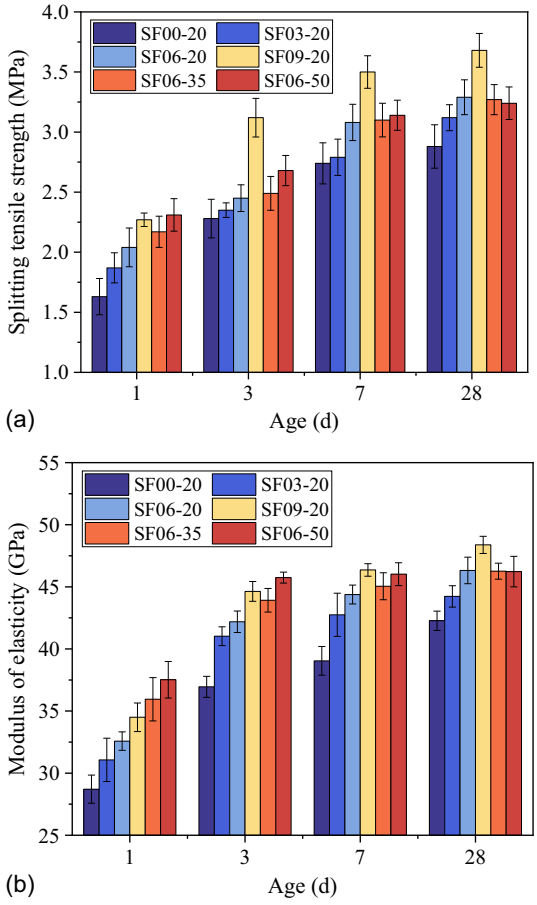

Fig. 5. (a) Splitting tensile strength of six mixtures; and (b) modulus of elasticity of six mixtures.

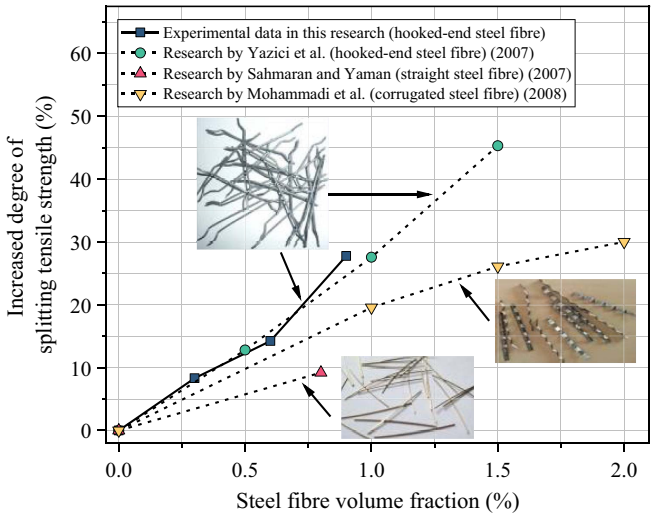

Fig. 6. Increased degree of splitting tensile strength with increasing contents of steel fibers in different shapes.

The hooked-end steel fiber showed a higher degree of enhancement in splitting tensile strength than other steel fibers in different shapes at similar steel fiber contents. Furthermore, despite potential discrepancies in concrete matrices across various experiments, it was observed that fibers of identical morphology consistently presented analogous enhancement trends. This underscores the importance of fiber shape in dictating tensile strength outcomes.

The 1-, 3-, and 7-day splitting tensile strength increased with increasing curing temperature at a steel fiber content of 0.6%. However, samples cured at 50°C exhibited a lower 28-day splitting tensile strength than those cured at 20°C. The results of Mixtures SF06-20, SF06-35, and SF06-50 reveal that elevating the curing temperature to 35°C and 50°C results in an enhancement of the initial strength development. However, it results in a decline in 28-day tensile strength. A possible explanation for these results may be that high-temperature curing has been observed to enhance the early-age tensile strength of concrete because of accelerated hydration reactions and subsequent initial strength gain. However, this strength improvement is primarily due to structural adjustments and hydration product formation. Over time, the influence of high-temperature curing diminishes, potentially resulting in the formation of large pore structures within the concrete. These pores can increase permeability, reduce the density of cementitious matrix, and potentially lead to lower tensile strength. (Jin et al. 2021).

Modulus of Elasticity

Fig. 5(b) depicts the results of the modulus of elasticity. The modulus of elasticity for all concrete mixtures increases with age. Fig. 5(b) shows that from 1 to 3 days, the modulus of elasticity in the concrete specimens increased rapidly. After 3 days, while the modulus continued to rise, the rate of increase slowed down. The initial rapid growth in the modulus of elasticity is largely due to the quick pace of chemical reactions during the early stages of cement hydration. The slower rate of increase after 3 days suggests that the initial rapid hydration process begins to taper off. As the most reactive cement particles have already combined with water to form the strength-giving hydrates, the remaining unhydrated cement reacts more slowly. Simultaneously, the growing crystalline structures within the concrete matrix make it harder for water to penetrate and sustain the hydration reaction. Furthermore, the concrete's internal structure becomes more stable, which naturally leads to a reduced capacity for further increases in stiffness and strength.

When the curing temperature was 20°C, the incorporation of steel fiber into the mixture led to an enhancement of the modulus of elasticity at all ages. The possible cause of this phenomenon might be that the incorporation of steel fibers leads to a decrease in the total cumulative pore volume and average pore diameter, resulting in denser and more compact concrete than concrete without steel fibers (Zheng et al. 2019). In addition, steel fiber has a higher modulus of elasticity than concrete, which may increase the modulus of elasticity of the composite. This phenomenon is typically due to the ability of the fibers to maintain their shape and distribute stress when subjected to force, thereby enhancing the overall modulus of elasticity of HSFRC. Therefore, the modulus of elasticity of HSFRC increased as steel fiber content increased.

The results show that an elevation in curing temperature significantly enhanced the modulus of elasticity at 1, 3, and 7 days. However, the values of the modulus of elasticity at 28 days were essentially consistent across different curing temperatures. For instance, the 3- or 28-day modulus of elasticity for Mixtures SF06-20, SF06-35, and SF06-50 was 42.19, 43.92, and 45.74 GPa or 46.32, 46.26, and 46.23 GPa, respectively. Elevating the curing temperature is known to accelerate the hydration reactions, which are crucial for the early strength and modulus of elasticity development in concrete. Faster hydration at higher temperatures promotes quicker formation and densification of the microstructure, thus enhancing the modulus of elasticity at 1, 3, and 7 days. The concrete at 28 days is likely to have reached a stage of relative maturation. At this point, the rate of hydration reactions has decelerated, and the microstructure has become more stable. This maturation leads to a stabilization in the values of the modulus of elasticity, thereby making the 28-day modulus of elasticity values essentially consistent across different curing temperatures.

Results of TSTM Test

The TSTM system was used to quantify the temperature process, total deformation strain, and restrained stress. Total deformation was obtained from free shrinkage specimen, while restrained stress was obtained from the restrained shrinkage specimen. Both specimens for the same mixture underwent the same curing mode.

Influence of Steel Fiber Content on Measured Curves

Fig. 7 depicts the results of the temperature process, restrained stress, and total deformation. Fig. 7(a) depicts that the pouring temperatures of Mixtures SF00-20, SF03-20, SF06-20, and SF09-20 were 25.44°C, 19.16°C, 20.17°C, and 21.83°C, respectively. The temperature of the HSFRC was adjusted to around 20°C within 1 h and then subjected to a constant-temperature curing process through the temperature control system. The four mixture specimens underwent a curing process at 20°C for 240 h, followed by a cooling process with a rate of 1.0°C/h until cracking occurred. The cracking temperature for Mixtures SF00-20, SF00-20, SF03-20, SF06-20, and SF09-20 was −5.38°C, −5.72°C, −7.79°C, and −14.02°C, respectively. As steel fiber content increased from 0 to 0.3%, 0.6%, and 0.9%, the cracking temperature decreased correspondingly.

The total deformation of HSFRC with varying contents of steel fibers is depicted in Fig. 7(b). In this research, the negative value of strain represents shrinkage, and the positive value represents expansion. The specimens of four mixtures exhibited small expansion deformation due to internal temperature rise at a very early age after pouring, and then gradually shrank because of the development of AS during the period of constant-temperature curing. The total deformation of HSFRC at 240 h for Mixtures SF06-20, SF06-35, and SF06-50 was −97, −86, −58, and −46 $\mu\varepsilon$, respectively. The magnitude of the total deformation decreased by 11.3%, 40.2%, and 52.6% as steel fiber content increased from 0 to 0.3%, 0.6%, and 0.9%. The reduction in deformation in the presence of steel fibers can be attributed to several factors. On one hand, steel fibers enhance the tensile strength of the concrete, which in turn reduces the extent of deformation under external loads or temperature variations. On the other hand, the fibers help in arresting the propagation of cracks that might occur because of shrinkage or thermal effects. By bridging the cracks, they provide a sort of "stitching" effect, which maintains the integrity of the material and reduces the deformation. During the cooling period, four specimens shrank rapidly until cracking.

Fig. 7(c) depicts the restrained stress of HSFRC. In this research, the positive value represents tensile stress, while the negative value represents compressive stress. The restrained stress of four concrete specimens developed slowly with the development of total deformation during the constant-temperature curing period, and then tensile stresses developed rapidly during the cooling period. Cracking stress for Mixtures SF00-20, SF03-20, SF06-20, and SF09-20 was 1.24 (at 265.58 h), 1.38 (at 269.15 h),

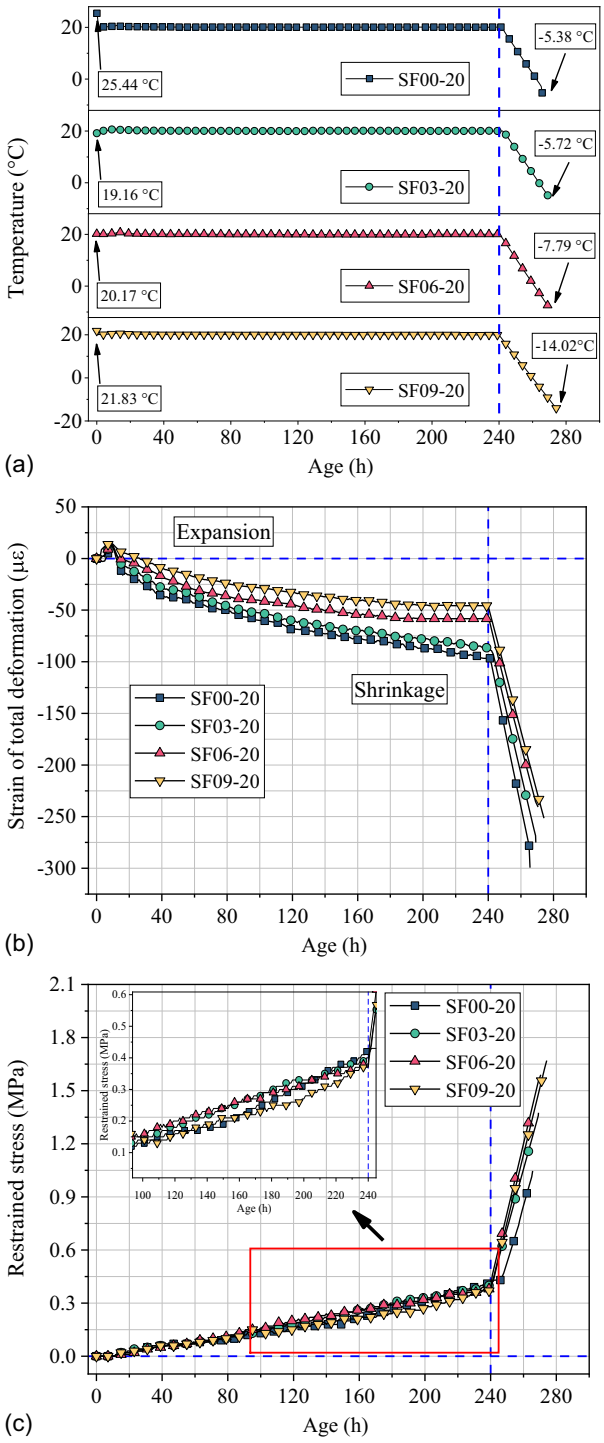

Fig. 7. (a) Temperature process; (b) total deformation; and (c) restrained stress of HSFRC with different steel fiber contents.

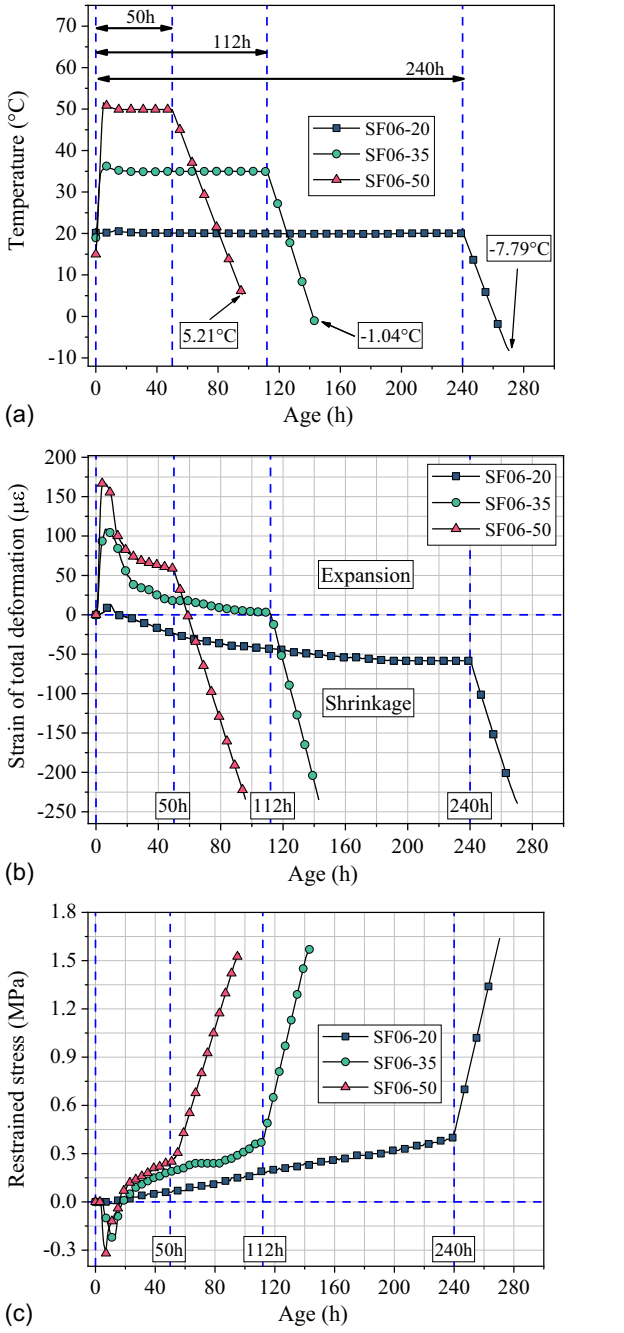

Fig. 8. (a) Temperature process; (b) total deformation; and (c) restrained stress of HSFRC at different curing temperatures.

1.59 (at 270.50 h), and 1.67 MPa (at 274.17 h), respectively. Cracking stress and cracking age both increased with increasing steel fiber content.

Influence of Curing Temperature on Measured Curves

Fig. 8 depicts the temperature process, total deformation, and restrained stress of HSFRC at different curing temperatures. Fig. 8(a) depicts that the pouring temperature for Mixtures SF06-20, SF06-35, and SF06-50 was 20.17°C, 18.95°C, and 14.98°C, respectively. Mixtures SF06-20, SF06-35, and SF06-50 were cured at 20°C, 35°C, and 50°C for 240, 112, and 50 h, respectively, and then cooled down with the same rate of 1.0°C/h until cracking occurred. The cracking temperature for Mixtures SF06-20, SF06-35, and SF06-50 was −7.79°C, −1.04°C, and 5.21°C, respectively. The cracking temperature increased with increasing curing temperature ranging from 20°C to 35°C and 50°C, respectively.

Fig. 8(b) depicts the total deformation of HSFRC at different curing temperatures. The specimens at different curing temperatures expanded first because of a temperature increase, then shrank during constant-temperature curing and cooling periods. The results of maximum expansion of HSFRC were 13, 126, and 178 $\mu\varepsilon$ for Mixtures SF06-20, SF06-35, and SF06-50, which increased significantly as curing temperature increased. The development rate of shrinkage was slow during the constant-temperature curing

J. Mater. Civ. Eng., 2024, 36(10): 04024293

period and accelerated significantly during the cooling period for three mixtures. The findings indicated that temperature variation significantly influenced the total deformation of concrete.

Fig. 8(c) depicts the restrained stress of HSFRC at different curing temperatures. The maximum compressive stress of Mixture SF06-20 was nearly 0, and the maximum compressive stress of Mixtures SF06-35 and SF06-50 was −0.24 and −0.32 MPa, respectively. A possible explanation might be that the concrete cured at higher temperatures has a higher modulus of elasticity and CTE (Zhao et al. 2019). During the cooling period, tensile stress experienced a rapid increase until cracking occurred. The cracking stress for Mixtures SF06-20, SF06-35, and SF06-50 was 1.64 MPa (at 270.50 h), 1.57 MPa (at 143.20 h), and 1.55 MPa (at 96.42 h), respectively. Hence, as curing temperature increased from 20°C to 35°C and 50°C, there was a corresponding decrease in both cracking stress and cracking age.

Early-Age AS of HSFRC

Influence of Steel Fiber Content on AS

Fig. 9 depicts AS results of Mixtures SF00-20, SF03-20, SF06-20, and SF09-20. The results showed that AS developed quickly during the initial hours after time-zero, and then the development rate of AS decreased gradually. Besides, the incorporation of steel fibers had a significant influence in reducing AS. For instance, AS at the cracking age of Mixtures SF00-20 (265.58 h) was −100, −90, −62, and −52 $\mu\varepsilon$ for Mixtures SF00-20, SF03-20, SF06-20, and SF09-20, respectively. The magnitude of AS decreased by 10.0%, 38.0%, and 48.0% as steel fiber contents increased from 0 to 0.3%, 0.6%, and 0.9%, respectively. AS was reduced by adding steel fiber, and the decreased degree compared with Mixture SF00-20 changed with time, as depicted in Fig. 9. The decreased degree of AS decreased rapidly in the initial phase and then gradually stabilized at a stable value. The stable value of the decreased degree compared with Mixture SF00-20 for Mixtures SF03-20, SF06-20, and SF09-20 was around 15%, 30%, and 45%, respectively. The reduction in the AS of concrete resulting from the addition of steel fiber can be attributed to the following reasons. First, steel fibers act as reinforcement within the concrete matrix, providing internal restraint against the volume changes that occur during the early stages of hydration. The internal restraint limits the movement and shrinkage of the cementitious matrix, reducing the AS of the concrete. Second, steel fibers enhance the tensile strength of concrete, which

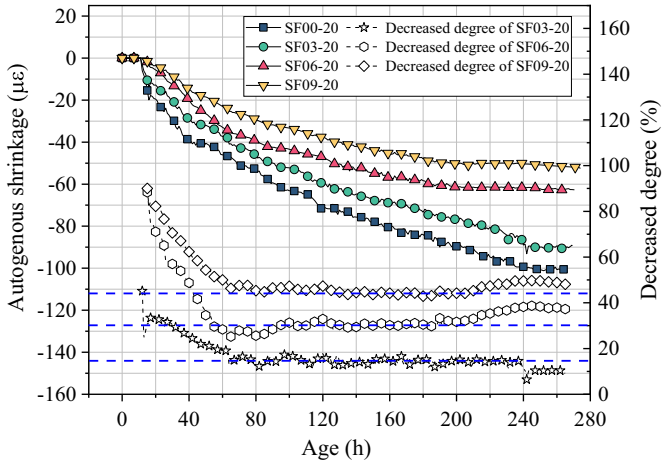

Fig. 9. AS of HSFRC with different steel fiber contents.

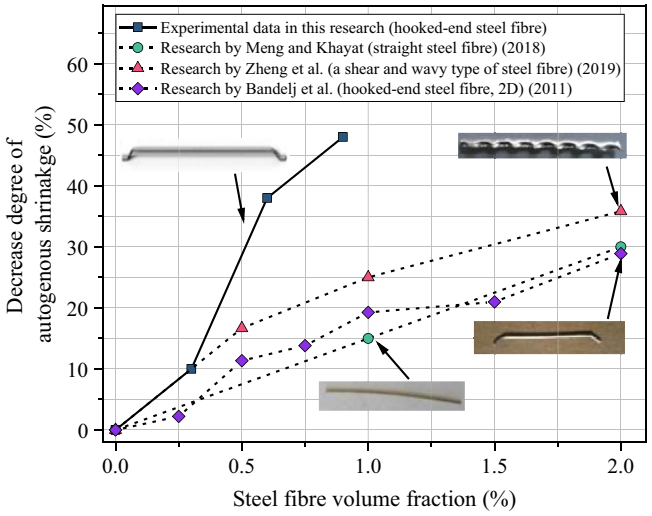

Fig. 10. Decreased degree of early-age autogenous shrinkage with increasing contents of steel fibers in different shapes.

helps to minimize the cracking and subsequent shrinkage of the concrete (Noushini et al. 2014). Therefore, AS was reduced effectively by adding steel fiber. A similar trend can be found in other studies concerning the AS of concrete reinforced with various contents of steel fibers (Bandelj et al. 2011; Meng and Khayat 2018; Miao et al. 2003; Zheng et al. 2019). Fig. 10 depicts the decreased degree of early-age AS with increasing contents of steel fibers in different shapes in Bandelj et al. (2011), Meng and Khayat (2018), and Zheng et al. (2019). To minimize the impact of the concrete matrix on the experimental results, the percentage reduction in AS with the addition of different shapes and contents of steel fibers was calculated based on the AS of the respective reference groups without steel fibers. The results revealed that within concrete, when incorporated at an identical content, hooked-end steel fibers used in this research exhibited superior shrinkage reduction efficiency, followed by shear and wavy types of steel fibers, while 2D hooked-end and straight steel fibers showed similar and comparatively lower efficiency. The 3D hooked ends of steel fibers enable better embedment in the concrete matrix, enhancing anchorage with the aggregate and cementitious matrix. This improved anchorage enhances the interaction between fibers and concrete, more effectively reducing the AS of concrete than the other types of steel fibers.

Influence of Curing Temperature on AS

Fig. 11 depicts the impact of curing temperature on the AS of HSFRC. All three mixtures show a rapid decrease in the early hours, suggesting a quick onset of AS. After the initial steep decline, the rate of shrinkage slows down for the mixtures cured under all temperatures. However, this deceleration occurs at different rates depending on the curing temperature. The findings revealed that a rise in curing temperature from 20°C to 35°C and 50°C results in a corresponding rise in the rate and magnitude of AS. The magnitude of AS at the cracking age of Mixture SF06-50 (96.42 h) increased by 123.3% and 134.9% as curing temperatures increased from 20°C to 35°C and 50°C. In addition, the average development rate of AS in the first 40 h after pouring for Mixtures SF06-20, SF06-35, and SF06-50 was −0.50, −1.92, and −2.41 $\mu\varepsilon$/h, respectively, the magnitude of which increased by 284.0% and 382.0% with increasing curing temperature. Similar trends regarding the effect of curing temperature on AS can be found in the study by Jiang et al. (2014). The temperature

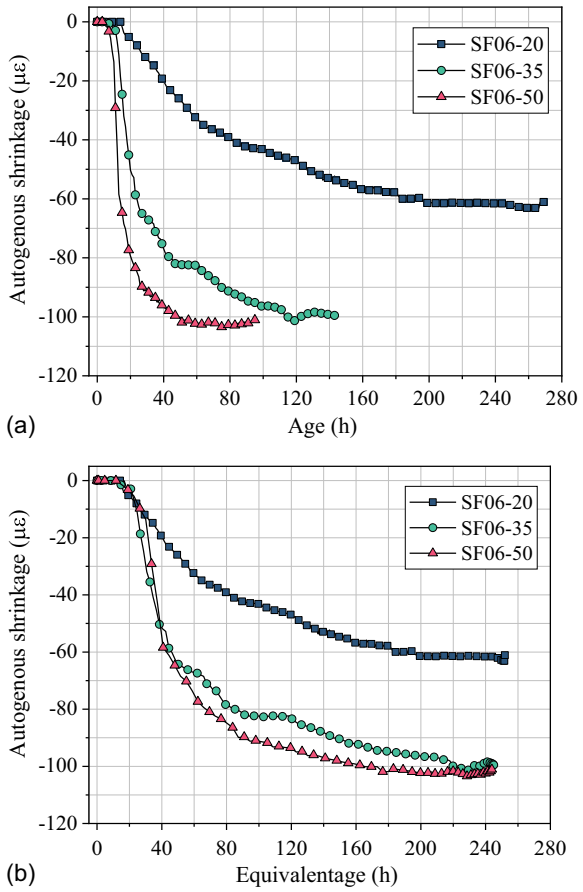

Fig. 11. AS of HSFRC at different curing temperatures: (a) evolution of AS with age; and (b) evolution of AS with equivalent age.

dependence of cement hydration and self-desiccation has contributed to the difference in the development rate of AS between the three mixtures (Sant 2012). The effect of curing temperature on the AS deformation of concrete is mainly achieved by affecting the rate of water evaporation and cement hydration inside concrete. When concrete is subjected to a higher curing temperature, the rate of water evaporation will accelerate, which will speed up the loss of water content inside the concrete and lead to an increase in AS deformation.

To better compare the AS of HSFRC at different curing temperatures, Fig. 11(b) depicts AS for Mixtures SF06-20, SF06-35, and SF06-50, which was maturity transformed by utilizing Eq. (1), as recommended by Sant (2012). The equivalent cracking age was 252.00, 245.04, and 244.16 h for Mixtures SF06-20, SF06-35, and SF06-50, respectively. However, AS curves in Fig. 11(b) at different curing temperatures were in different patterns. For instance, the development rate of AS was different for three mixtures in the first few hours after time-zero, and the AS of concrete at the equivalent age of 244 h for Mixtures SF06-20, SF06-35, and SF06-50 was −62, −99, and −102 $\mu\varepsilon$, respectively. The results indicated that maturity transformation failed to describe the temperature-dependent deformation processes. The curing temperature would influence the cement hydration rate, internal relative humidity, and microstructural arrangement of the system, which might cause the difference between the AS of Mixtures SF06-20, SF06-35, and SF06-50 at the equivalent age (Lothenbach et al. 2008). Therefore, although the maturity concept can be utilized to predict the degree of reaction, it fails to describe the process of AS of concrete at different curing temperatures.

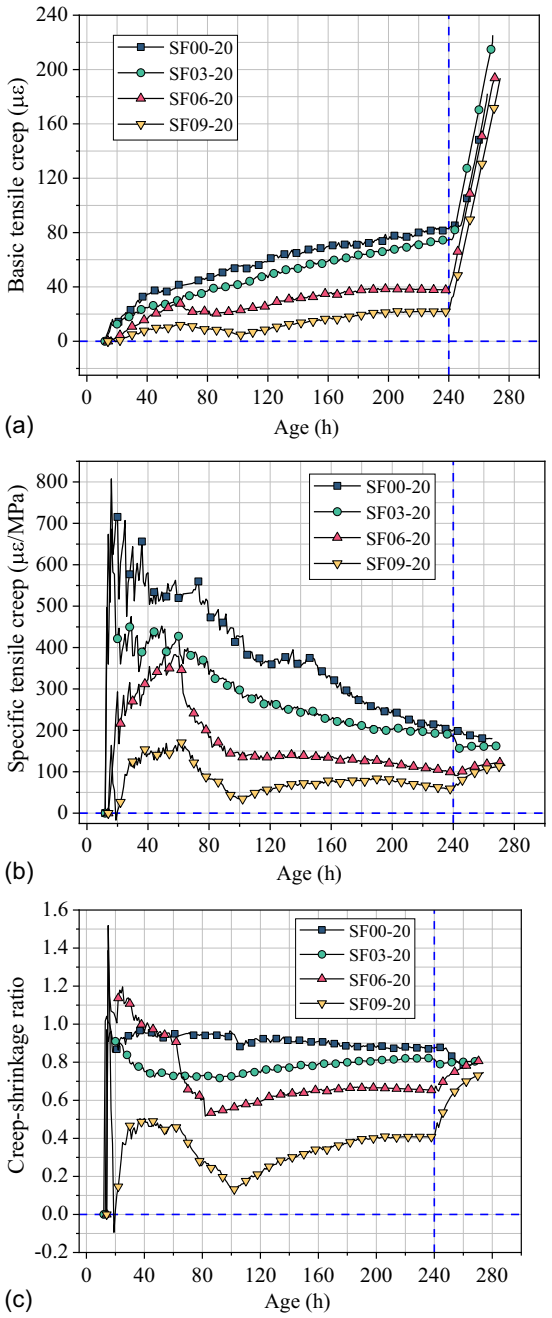

Fig. 12. (a) Basic TC; (b) specific TC; and (c) creep–shrinkage ratio of HSFRC with different steel fiber contents.

Early-Age TC Behavior of HSFRC

Influence of Steel Fiber Content on TC Behavior

Fig. 12 depicts the basic TC, specific TC, and creep–shrinkage ratio of HSFRC with different steel fiber contents. Basic TC was established based on the point at which restrained tensile stress occurred. The creep behavior is affected by numerous factors, including temperature process and restrained stress (Zhang and Qin 2006). AS of concrete developed quickly during the constant temperature curing period, leading to the development of tensile stress in concrete. The thermal shrinkage that occurred during the cooling period would further increase the tensile stress. All the mixtures exhibit a similar trend: a gradual increase in TC with time. There is a slight acceleration in the creep rate after approximately 120 h

for all specimens. The incorporation of steel fibers reduced the basic TC during the constant-temperature curing period. For instance, the basic TC at 240 h for Mixtures SF00-20, SF03-20, SF06-20, and SF09-20 was 83, 73, 38, and 22 $\mu\varepsilon$, which decreased by 12%, 54.2%, and 73.5% as steel fiber content increased from 0 to 0.3%, 0.6%, and 0.9%, respectively.

Fig. 12(b) depicts the curves of specific TC. The specific creep varied greatly in the initial phase, then decreased gradually and stabilized at a stable value. Similar trends are reported in the study (Zhao et al. 2019). The findings showed that the specific TC decreased as steel fiber content increased. Fig. 12(c) depicts the curves of creep–shrinkage ratio. The creep–shrinkage ratio decreased with increasing steel fiber content during the constant-temperature curing period. The result reveals a decrease in the degree of stress relaxation by adding steel fibers.

The results showed a significant decrease in the basic TC, specific TC, and creep–shrinkage ratio by adding steel fibers, indicating that the incorporation of steel fiber effectively reduced the TC behavior of HSFRC. A possible explanation for these results may be that the presence of steel fibers increases the frictional resistance between the fiber and the surrounding matrix. The enhanced frictional interaction contributes to improved load transfer and reduces the potential for creep deformation. In addition, the influence of internal restrain increases with increasing steel fiber content. The restraint limits the development of microcracks and reduces the TC response of the concrete over time. With an increase in steel fiber content, there is a corresponding enhancement in the concrete matrix's microstructure. This enhancement is crucial for effective load transfer, which mitigates the creep phenomenon. Moreover, the physical integration of steel fibers within the concrete serves as a blockade to the matrix's movement, thereby impeding the advancement of creep. The presence of these fibers throughout the concrete leads to a synergistic composite effect, bolstering the material's capacity to withstand prolonged tensile stresses without significant deformation.

Influence of Curing Temperature on TC Behavior

The basic TC, specific TC, and creep-shrinkage ratio of HSFRC at different curing temperatures are depicted in Fig. 13. The analysis was performed at the same equivalent age to study the influence of curing temperature. Fig. 13(a) depicts that an increase in curing temperature increased the basic TC. For instance, the basic TC at the equivalent age of 160 h for Mixtures SF06-20, SF06-35, and SF06-50 was 35, 89, and 98 $\mu\varepsilon$, which increased by 154.3%, and 180.0% as curing temperature increased from 20°C to 35°C and 50°C, respectively. In addition, the initial basic creep rate of HSFRC significantly increased as the curing temperature increased, particularly when the curing temperature increased from 20°C to 35°C. Fig. 13(a) depicts that the difference between the initial basic creep rate of HSFRC cured at 35°C and 50°C was small. Vu et al. (2012) also observed that creep was enhanced at higher curing temperatures.

Fig. 13(b) depicts the curves of specific TC at different curing temperatures. Considering that the specific creep varied greatly in the early stage because the values of the restrained stress were small, the curves of the specific creep in the early stage are not depicted in Fig. 13(b). The results of specific TC depicted in Fig. 13(b) indicated that the specific TC increased with increasing curing temperature, and the specific TC decreased gradually with increasing equivalent age. For instance, the restrained stress at the equivalent age of 160 h was 0.26, 0.24, and 0.18 MPa, and the specific TC at that time was 134.62, 370.83, and 544.44 $\mu\varepsilon$/MPa for Mixtures SF06-20, SF06-35, and SF06-50, which increased by 175.5% and 304.4% with increasing curing temperature ranging from 20°C to 35°C and 50°C, respectively. An increase in specific TC is observed initially because of the microstructural instability induced by ongoing hydration reactions in the freshly cast concrete. As hydration proceeds, the microstructure is stabilized through the filling of pores by hydration products, leading to enhanced stiffness and density of the concrete matrix. Consequently, a reduction in specific TC is observed. With the increase of the equivalent age, the microstructure of concrete is further stabilized and strengthened through continued hydration, resulting in a gradual reduction of specific TC.

Fig. 13(c) depicts the curves of creep–shrinkage ratio. The creep–shrinkage ratio increased as the curing temperature increased.

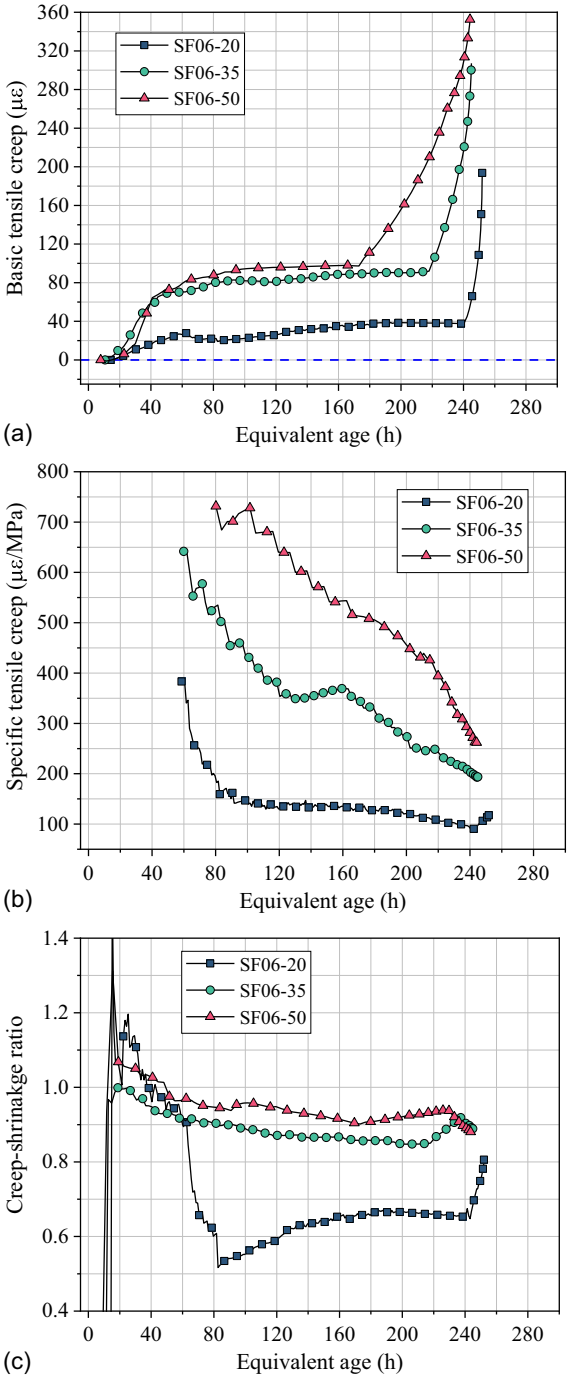

Fig. 13. (a) Basic TC; (b) specific TC; and (c) creep–shrinkage ratio of HSFRC at different curing temperatures.

For instance, the free shrinkage at the equivalent age of 160 h was 54, 102, and 107 $\mu\varepsilon$, and the creep–shrinkage ratio at that time was 0.65, 0.87, and 0.92 for Mixtures SF06-20, SF06-35, and SF06-50, which increased by 33.8% and 41.5% as curing temperature increased from 20°C to 35°C and 50°C, respectively. The result demonstrates that the thermal treatment increased the degree of stress relaxation.

High curing temperature would accelerate the break and restoration of the bond between nanostructure layers in concrete, leading to an increase in concrete creep. However, an increase in curing temperature also promotes cement hydration and increases stiffness of the concrete, thus theoretically reducing concrete creep. From the results of basic TC depicted in Fig. 13(a), it was observed that the increase in creep outweighed the increase in stiffness as the curing temperature increased, leading to an overall increase in basic TC as the curing temperature increased. In addition, an increase in curing temperature led to an increase in AS of HSFRC. A greater magnitude of shrinkage may cause greater TC in concrete under restrained condition (Zhang and Qin 2006). As the AS increased, the frequency of repositioning of the concrete specimen under restrained conditions rose, generating numerous microcracks within the concrete. The occurrence of these microcracks fosters the development of TC as they provide room for deformation and potential release of internal stresses (Altoubat and Lange 2001).

Evaluation of the Early-Age Cracking Potential of HSFRC

Cracking Age, Cracking Temperature, and Cracking Stress

The cracking potential of concrete under various test conditions is evaluated using quantitative criteria related to TSTM. Single criterion and integrated criteria, i.e., cracking age, cracking temperature, cracking stress, restrained stress–to–tensile strength ratio, and stress reserve, were used to evaluate the early-age cracking behavior of HSFRC in this research, as recommended by Shen et al. (2020). Table 3 depicts the results of single criterion on HSFRC.

When steel fiber content increased, the HSFRC showed an increase in both cracking age and cracking stress, while the cracking temperature decreased. The results revealed that the HSFRC with a steel fiber content of 0.9% exhibited the least cracking potential at early age when the curing temperature was maintained at 20°C. However, when the curing temperature increased, the results of single criterion showed an opposite trend.

Restrained Stress–to–Tensile Strength Ratio

Concrete is expected to crack when a combination of the elastic modulus and the shrinkage strain induces a stress level that exceeds its tensile strength (Mehta and Monteiro 2014). Thus, the cracking potential of concrete was assessed using the restrained stress–to–tensile strength ratio in numerous studies (Igarashi et al. 2000; Riding et al. 2008), which was obtained based on the restrained stress and the axial tensile strength predicted by prediction models. The axial tensile strength can be estimated using Eqs. (10) and (11) (Kanstad et al. 2003a, b). Concrete often experiences cracking when the restrained stress–to–strength ratio is below 1, primarily due to the presence of microcracks. These microcracks exist within the concrete matrix even before any external load is applied. When under stress, the existing small flaws in concrete serve as points where stress is concentrated. This means that the stress around these small flaws becomes higher. As a result, even if the restrained stress–to–strength ratio in the concrete is below 1, the increased stress at the locations of these small flaws might go beyond the concrete's ability to resist tearing, which can lead to the spread of cracks

$$f_t = 0.77 \times f_{spl} + 0.21 \tag{10}$$

$$f_t(t) = f_{t,28} \exp\{-\lambda_1[\ln(1 + (t - t_0))]^{-k_1}\} \tag{11}$$

where f_t = axial tensile strength, in MPa; f_{spl} = splitting tensile strength, in MPa; $f_t(t)$ = time-dependent axial tensile strength, in MPa; $f_{t,28}$ = 28-d axial tensile strength, in MPa; and λ_1, k_1 = fitting parameters.

Table 3. Cracking age, cracking temperature, and cracking stress of HSFRC

Mixture	Cracking age (h)	Cracking temperature (°C)	Cracking stress (MPa)
SF00-20	265.58	−5.38	1.24
SF03-20	269.15	−5.72	1.38
SF06-20	270.50	−7.79	1.59
SF09-20	274.17	−14.02	1.67
SF06-35	143.20	−1.04	1.57
SF06-50	96.42	5.21	1.35

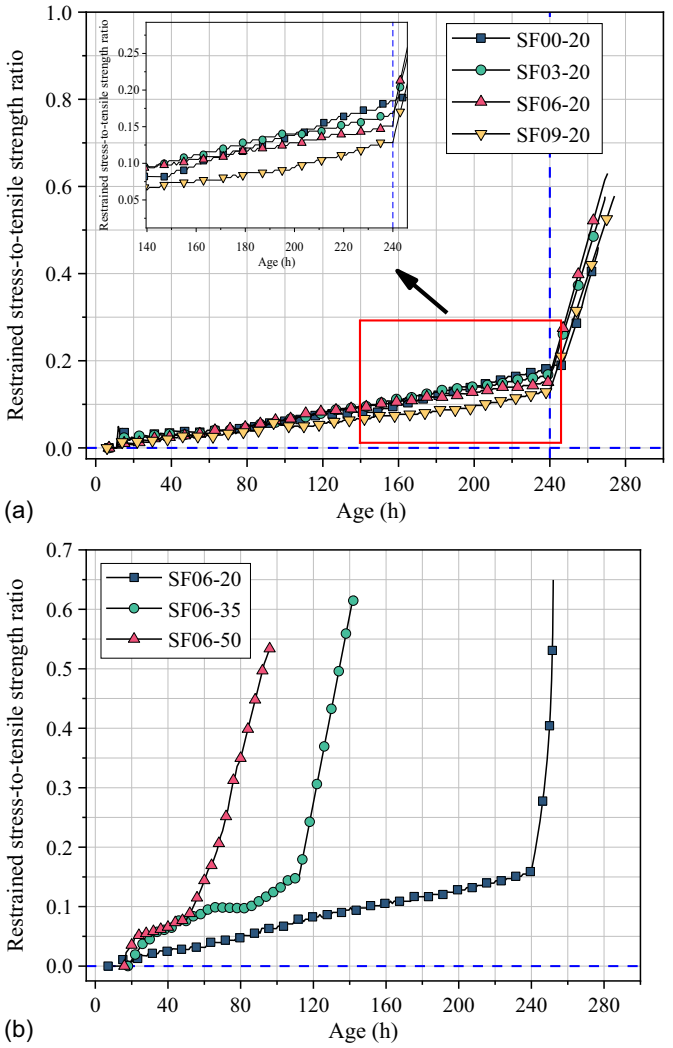

Fig. 14. Restrained stress–to–tensile strength ratio of HSFRC: (a) with different steel fiber contents; and (b) at different curing temperatures.

Fig. 14 depicts the evolution of the restrained stress–to–tensile strength ratio. During the constant temperature curing period, the restrained stress–to–tensile strength ratio of six mixtures showed a gradual increase over time and increased rapidly during the cooling period, which indicated that the rapid cooling was not conducive to the cracking resistance of HSFRC.

Fig. 14(a) depicts that the restrained stress–to–tensile strength ratio decreased as steel fiber content increased during the constant-temperature curing period. For instance, the restrained stress–to–tensile strength ratio at 240 h was 0.185, 0.168, 0.151, and 0.128 for Mixtures SF00-20, SF03-20, SF06-20, and SF09-20, which decreased by 9.2%, 18.4%, and 30.8% as steel fiber content increased from 0 to 0.3%, 0.6%, and 0.9%, respectively. The lower ratio represents the higher cracking resistance of concrete. Thus, the HSFRC with more steel fiber content had lower cracking potential.

The restrained stress–to–tensile strength ratio of HSFRC at different curing temperatures is depicted in Fig. 14(b). During the constant-temperature curing period, the ratios of HSFRC cured at 35°C and 50°C were higher than that of HSFRC cured at 20°C. However, there was little difference between the ratios of HSFRC cured at 35°C and 50°C. The findings indicated that an increase in curing temperature increased the early-age cracking potential of HSFRC.

Stress Reserve

The stress at room temperature for Mixtures SF00-20, SF03-20, SF06-20, SF09-20, SF06-35, and SF06-50 was −0.41, −0.44, −0.42, −0.39, −0.89, and −0.88 MPa, respectively. Fig. 15 depicts the results of the stress reserve of HSFRC at early age.

As depicted in Fig. 15, the stress reserve of HSFRC increased by 1.5%, 10.4%, and 14.9% as steel fiber content increased from 0 to 0.3%, 0.6%, and 0.9%, and decreased by 41.9% and 52.7% as curing temperature increased from 20°C to 35°C and 50°C, respectively. The findings showed that a higher stress reserve corresponds to a lower cracking potential (Shi et al. 2014). Thus, the incorporation of steel fibers significantly decreased the cracking potential of HSFRC cured under 20°C. First, steel fibers enhance the internal tensile capacity of the concrete, helping to resist tensile stresses caused by external loads or changes in internal stress. Second, the network of steel fibers within the concrete can effectively bridge microcracks, limiting their development and spread, thereby reducing the likelihood of crack formation. Third, steel fibers improve the distribution of stress within the concrete, making it more uniform and reducing the occurrence of cracks due to stress concentration.

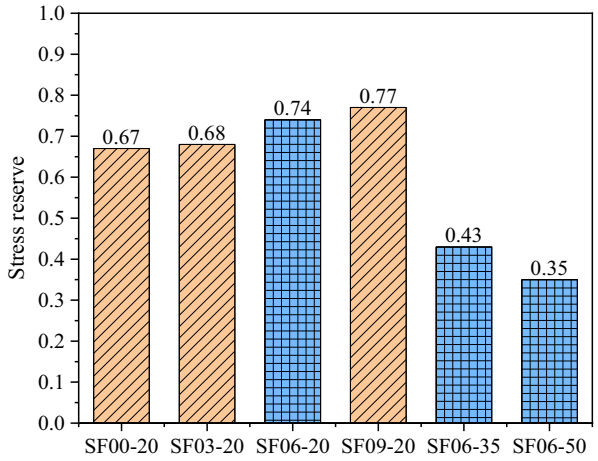

Fig. 15. Stress reserve of HSFRC.

However, an increase in curing temperature increased the cracking potential of HSFRC with the same steel fiber content. Higher temperatures can accelerate the hydration reaction within concrete, but this may lead to uneven hydration levels within the material. The surface layer can dry out rapidly because of the swift loss of moisture, while the interior remains moist. Such unevenness can result in the accumulation of internal stress, increasing the risk of internal damage and the formation of cracks. Additionally, the accelerated pace of hydration under higher temperature curing conditions may disrupt the orderly formation of the concrete's microstructure, reducing the stability of the early-age microstructure. This can make the concrete more susceptible to microdamage under the influence of external forces or internal stresses, which can then develop into macroscopic cracks.

Conclusion

The influences of different steel fiber contents and curing temperatures on mechanical properties, temperature process, restrained stress, AS, TC, and cracking behavior of HSFRC were investigated and presented in this research. The main conclusions based on the experimental data are as follows:

An increase in curing temperature increased the cracking potential of HSFRC with the same steel fiber content. The short-term benefits of elevated temperatures were evident as the 1-, 3-, and 7-day splitting tensile strength and modulus of elasticity improved because of faster cement hydration reactions. However, the 28-day splitting tensile strength decreased with increasing curing temperature, and the modulus of elasticity values at 28 days were essentially consistent across different curing temperatures. Furthermore, an increase from 20°C to 35°C and 50°C significantly increased the rate and magnitude of AS. Besides, the basic TC, specific TC, and creep–shrinkage ratio increased with increasing curing temperature.

The cracking potential of HSFRC under uniaxial constant restrained condition decreased with increasing steel fiber content. An increase in steel fiber content led to an increase in both splitting tensile strength and modulus of elasticity of HSFRC. Additionally, as the steel fiber content increased, there was a notable decrease in AS, basic TC, specific TC, and creep–shrinkage ratio of HSFRC, thus enhancing the structural integrity and durability of the concrete under constant-temperature curing conditions. These improvements indicate that steel fibers can play a crucial role in improving both the mechanical properties and the long-term serviceability of concrete.

Maximizing steel fiber content within cost-effective bounds and choosing an ideal curing temperature are key to achieving a balanced enhancement in mechanical properties, cracking resistance, and overall material performance. Additional research is needed to establish the optimal ranges of steel fiber content and curing temperature for improved performance of HSFRC.

Data Availability Statement

All data, models, and code generated or used during the study appear in the published article.

Acknowledgments

The support of the Fundamental Research Funds for the Central Universities (Grant No. B230201060) is gratefully acknowledged.

References

Abdallah, S., M. Fan, and K. A. Cashell. 2017. "Pull-out behaviour of straight and hooked-end steel fibres under elevated temperatures." *Cem. Concr. Res.* 95 (May): 132–140. https://doi.org/10.1016/j.cemconres.2017.02.010.

Abdallah, S., M. Fan, and D. W. A. Rees. 2016. "Analysis and modelling of mechanical anchorage of 4D/5D hooked end steel fibres." *Mater. Des.* 112 (Dec): 539–552. https://doi.org/10.1016/j.matdes.2016.09.107.

Abdallah, S., D. W. A. Rees, S. H. Ghaffar, and M. Fan. 2018. "Understanding the effects of hooked-end steel fibre geometry on the uniaxial tensile behaviour of self-compacting concrete." *Constr. Build. Mater.* 178 (Jul): 484–494. https://doi.org/10.1016/j.conbuildmat.2018.05.191.

Afroughsabet, V., L. Biolzi, and T. Ozbakkaloglu. 2016. "High-performance fiber-reinforced concrete: A review." *J. Mater. Sci.* 51 (14): 6517–6551. https://doi.org/10.1007/s10853-016-9917-4.

Alrawashdeh, A., and O. Eren. 2022. "Mechanical and physical characterisation of steel fibre reinforced self-compacting concrete: Different aspect ratios and volume fractions of fibres." *Results Eng.* 13 (Mar): 100335. https://doi.org/10.1016/j.rineng.2022.100335.

Altoubat, S. A., and D. A. Lange. 2001. "Creep, shrinkage, and cracking of restrained concrete at early age." *ACI Mater. J.* 98 (4): 323–331.

ASTM. 2020. *Standard specification for portland cement*. ASTM C150/C150M-20. West Conshohocken, PA: ASTM.

Bandelj, B., D. Saje, J. Šušteršič, J. Lopatič, and F. Saje. 2011. "Free shrinkage of high performance steel fiber reinforced concrete." *J. Test. Eval.* 39 (2): 166–176. https://doi.org/10.1520/JTE103028.

Barros, J. A. O., V. M. C. F. Cunha, A. F. Ribeiro, and J. A. B. Antunes. 2005. "Post-cracking behaviour of steel fibre reinforced concrete." *Mater. Struct.* 38 (1): 47–56. https://doi.org/10.1007/BF02480574.

Bentur, A. 2001. "Early-age shrinkage and cracking in cementitious systems." *Concr. Sci. Eng.* 3 (Mar): 3–12.

Bentz, D. P., and K. A. Snyder. 1999. "Protected paste volume in concrete: Extension to internal curing using saturated lightweight fine aggregate." *Cem. Concr. Res.* 29 (11): 1863–1867. https://doi.org/10.1016/S0008-8846(99)00178-7.

Bissonnette, B., and M. Pigeon. 1995. "Tensile creep at early ages of ordinary, silica fume and fiber reinforced concretes." *Cem. Concr. Res.* 25 (5): 1075–1085. https://doi.org/10.1016/0008-8846(95)00102-I.

Bloom, R., and A. Bentur. 1993. "Restrained shrinkage of high strength concrete." In Vol. 2 of *Proc., Symp. on Utilization of High Strength Concrete*, 1007–1014. Oslo, Norway: Norsk betongforening.

Chen, M., H. Zhong, and M. Zhang. 2020. "Flexural fatigue behaviour of recycled tyre polymer fibre reinforced concrete." *Cem. Concr. Compos.* 105 (Jan): 103441. https://doi.org/10.1016/j.cemconcomp.2019.103441.

Chinese Standard. 2018. *Common portland cement*. [In Chinese.] GB 175-2007/XG1-2018. Beijing: Standard Press of China.

Chinese Standard. 2019. *Standard for test methods of concrete physical and mechanical properties*. [In Chinese.] GB/T 50081-2019. Beijing: Standard Press of China.

Chu, I., S. H. Kwon, M. N. Amin, and J.-K. Kim. 2012. "Estimation of temperature effects on autogenous shrinkage of concrete by a new prediction model." *Constr. Build. Mater.* 35 (Oct): 171–182. https://doi.org/10.1016/j.conbuildmat.2012.03.005.

Cusson, D., and T. Hoogeveen. 2007. "An experimental approach for the analysis of early-age behaviour of high-performance concrete structures under restrained shrinkage." *Cem. Concr. Res.* 37 (2): 200–209. https://doi.org/10.1016/j.cemconres.2006.11.005.

Darquennes, A., S. Staquet, and B. Espion. 2011. "Determination of time-zero and its effect on autogenous deformation evolution." *Eur. J. Environ. Civ. Eng.* 15 (7): 1017–1029. https://doi.org/10.1080/19648189.2011.9695290.

Da Silva, C. A. N., J. Ciambella, J. A. O. Barros, and I. G. Costa. 2020. "A model for optimizing hooked end steel fibre reinforcements in cracked cement composites." *Appl. Eng. Sci.* 3 (Sep): 100011. https://doi.org/10.1016/j.apples.2020.100011.

Frazão, C., J. Barros, J. A. Bogas, V. García-Cortés, and T. Valente. 2022. "Technical and environmental potentialities of recycled steel fiber reinforced concrete for structural applications." *J. Build. Eng.* 45 (Jan): 103579. https://doi.org/10.1016/j.jobe.2021.103579.

Garas, V. Y., L. F. Kahn, and K. E. Kurtis. 2009. "Short-term tensile creep and shrinkage of ultra-high performance concrete." *Cem. Concr. Compos.* 31 (3): 147–152. https://doi.org/10.1016/j.cemconcomp.2009.01.002.

Garas, V. Y., K. E. Kurtis, and L. F. Kahn. 2012. "Creep of UHPC in tension and compression: Effect of thermal treatment." *Cem. Concr. Compos.* 34 (4): 493–502. https://doi.org/10.1016/j.cemconcomp.2011.12.002.

Guzlena, S., and G. Sakale. 2021. "Self-healing of glass fibre reinforced concrete (GRC) and polymer glass fibre reinforced concrete (PGRC) using crystalline admixtures." *Constr. Build. Mater.* 267 (Jan): 120963. https://doi.org/10.1016/j.conbuildmat.2020.120963.

Haddad, R. H., and M. M. Smadi. 2004. "Role of fibers in controlling unrestrained expansion and arresting cracking in portland cement concrete undergoing alkali–silica reaction." *Cem. Concr. Res.* 34 (1): 103–108. https://doi.org/10.1016/S0008-8846(03)00245-X.

Hauggaard, A. B., L. Damkilde, and P. F. Hansen. 1999. "Transitional thermal creep of early age concrete." *J. Eng. Mech.* 125 (4): 458–465. https://doi.org/10.1061/(ASCE)0733-9399(1999)125:4(458).

Huang, H., and G. Ye. 2017. "Examining the 'time-zero' of autogenous shrinkage in high/ultra-high performance cement pastes." *Cem. Concr. Res.* 97 (Jul): 107–114. https://doi.org/10.1016/j.cemconres.2017.03.010.

Hubert, M., C. Desmettre, and J.-P. Charron. 2014. "Influence of fiber content and reinforcement ratio on the water permeability of reinforced concrete." *Mater. Struct.* 48 (9): 2795–2807. https://doi.org/10.1617/s11527-014-0354-z.

Igarashi, S., A. Bentur, and K. Kovler. 2000. "Autogenous shrinkage and induced restraining stresses in high-strength concretes." *Cem. Concr. Res.* 30 (11): 1701–1707. https://doi.org/10.1016/S0008-8846(00)00399-9.

Jiang, C., Y. Yang, Y. Wang, Y. Zhou, and C. Ma. 2014. "Autogenous shrinkage of high performance concrete containing mineral admixtures under different curing temperatures." *Constr. Build. Mater.* 61 (Jun): 260–269. https://doi.org/10.1016/j.conbuildmat.2014.03.023.

Jin, W., L. Jiang, L. Han, L. Chen, X. Yan, and C. Chen. 2021. "Influence of curing temperature on the mechanical properties and microstructure of limestone powder mass concrete." *Struct. Concr.* 22 (Jan): E745–E755. https://doi.org/10.1002/suco.201900549.

Kalpana, M., and A. Tayu. 2020. "Light weight steel fibre reinforced concrete: A review." *Mater. Today: Proc.* 22 (Jan): 884–886. https://doi.org/10.1016/j.matpr.2019.11.095.

Kang, J., D. Shen, C. Liu, M. Li, C. Wen, and X. Shi. 2023. "Early-age autogenous shrinkage and cracking risk of 5D hooked-end steel fiber–reinforced high-strength concrete under uniaxial restrained condition." *J. Mater. Civ. Eng.* 35 (8): 04023220. https://doi.org/10.1061/JMCEE7.MTENG-15446.

Kanstad, T., T. A. Hammer, Ø. Bjøntegaard, and E. J. Sellevold. 2003a. "Mechanical properties of young concrete: Part I: Experimental results related to test methods and temperature effects." *Mater. Struct.* 36 (4): 218–225. https://doi.org/10.1007/BF02479614.

Kanstad, T., T. A. Hammer, Ø. Bjøntegaard, and E. J. Sellevold. 2003b. "Mechanical properties of young concrete: Part II: Determination of model parameters and test program proposals." *Mater. Struct.* 36 (4): 226–230. https://doi.org/10.1007/BF02479615.

Kolver, K., S. Igarashi, and A. Bentur. 1999. "Tensile creep behavior of high strength concretes at early ages." *Mater. Struct.* 32 (5): 383–387. https://doi.org/10.1007/BF02479631.

Kovler, K. 1994. "Testing system for determining the mechanical behaviour of early age concrete under restrained and free uniaxial shrinkage." *Mater. Struct.* 27 (6): 324–330. https://doi.org/10.1007/BF02473424.

Lee, Y., S.-T. Yi, M.-S. Kim, and J.-K. Kim. 2006. "Evaluation of a basic creep model with respect to autogenous shrinkage." *Cem. Concr. Res.* 36 (7): 1268–1278. https://doi.org/10.1016/j.cemconres.2006.02.011.

Li, M., D. Shen, Q. Yang, X. Cao, C. Liu, and J. Kang. 2022. "Rehabilitation of seismic-damaged reinforced concrete beam-column joints with different corrosion rates using basalt fiber–reinforced polymer sheets." *Compos. Struct.* 289 (Jun): 115397. https://doi.org/10.1016/j.compstruct.2022.115397.

Liu, R., H. Xiao, J. Geng, J. Du, and M. Liu. 2020. "Effect of nano-$CaCO_3$ and nano-SiO_2 on improving the properties of carbon fibre-reinforced concrete and their pore-structure models." *Constr. Build. Mater.* 244 (May): 118297. https://doi.org/10.1016/j.conbuildmat.2020.118297.

Lothenbach, B., T. Matschei, G. Möschner, and F. P. Glasser. 2008. "Thermodynamic modelling of the effect of temperature on the hydration and porosity of portland cement." *Cem. Concr. Res.* 38 (1): 1–18. https://doi.org/10.1016/j.cemconres.2007.08.017.

Lura, P., K. Van Breugel, and I. Maruyama. 2001. "Effect of curing temperature and type of cement on early-age shrinkage of high-performance concrete." *Cem. Concr. Res.* 31 (12): 1867–1872. https://doi.org/10.1016/S0008-8846(01)00601-9.

Meddah, M. S., and A. Tagnit-Hamou. 2011. "Evaluation of rate of deformation for early-age concrete shrinkage analysis and time zero determination." *J. Mater. Civ. Eng.* 23 (7): 1076–1086. https://doi.org/10.1061/(ASCE)MT.1943-5533.0000261.

Mehta, P. K., and P. J. M. Monteiro. 2014. *Concrete: Microstructure, properties, and materials*. New York: McGraw-Hill.

Meng, W., and K. H. Khayat. 2018. "Effect of hybrid fibers on fresh properties, mechanical properties, and autogenous shrinkage of cost-effective UHPC." *J. Mater. Civ. Eng.* 30 (4): 04018030. https://doi.org/10.1061/(ASCE)MT.1943-5533.0002212.

Miao, B., J.-C. Chern, and C.-A. Yang. 2003. "Influences of fiber content on properties of self-compacting steel fiber reinforced concrete." *J. Chin. Inst. Eng.* 26 (4): 523–530. https://doi.org/10.1080/02533839.2003.9670805.

Mohammadi, Y., S. P. Singh, and S. K. Kaushik. 2008. "Properties of steel fibrous concrete containing mixed fibres in fresh and hardened state." *Constr. Build. Mater.* 22 (5): 956–965. https://doi.org/10.1016/j.conbuildmat.2006.12.004.

Murugan, K., S. J. Stephen, and R. Gettu. 2020. "Influence of fibre geometry on the fracture of steel fibre reinforced concrete." *IOP Conf. Ser.: Mater. Sci. Eng.* 936 (1): 012025. https://doi.org/10.1088/1757-899X/936/1/012025.

Nataraja, M., N. Dhang, and A. Gupta. 1999. "Stress–strain curves for steel-fiber reinforced concrete under compression." *Cem. Concr. Compos.* 21 (5–6): 383–390. https://doi.org/10.1016/S0958-9465(99)00021-9.

Noushini, A., K. Vessalas, G. Arabian, and B. Samali. 2014. "Drying shrinkage behaviour of fibre reinforced concrete incorporating polyvinyl alcohol fibres and fly ash." *Adv. Civ. Eng.* 2014 (May): 1–10. https://doi.org/10.1155/2014/836173.

Riding, K. A., J. L. Poole, A. K. Schindler, M. C. Juenger, and K. J. Folliard. 2008. "Quantification of effects of fly ash type on concrete early-age cracking." *ACI Mater. J.* 105 (2): 149–155.

Sahmaran, M., M. Al-Emam, G. Yıldırım, Y. E. Şimşek, T. K. Erdem, and M. Lachemi. 2015. "High-early-strength ductile cementitious composites with characteristics of low early-age shrinkage for repair of infrastructures." *Mater. Struct.* 48 (5): 1389–1403. https://doi.org/10.1617/s11527-013-0241-z.

Sahmaran, M., and I. O. Yaman. 2007. "Hybrid fiber reinforced self-compacting concrete with a high-volume coarse fly ash." *Constr. Build. Mater.* 21 (1): 150–156. https://doi.org/10.1016/j.conbuildmat.2005.06.032.

Sant, G. 2012. "The influence of temperature on autogenous volume changes in cementitious materials containing shrinkage reducing admixtures." *Cem. Concr. Compos.* 34 (7): 855–865. https://doi.org/10.1016/j.cemconcomp.2012.04.003.

Sellevold, E. J., and Ø. Bjøntegaard. 2006. "Coefficient of thermal expansion of cement paste and concrete: Mechanisms of moisture interaction." *Mater. Struct.* 39 (9): 809–815. https://doi.org/10.1617/s11527-006-9086-z.

Shao, R., C. Wu, J. Li, and Z. Liu. 2022. "Development of sustainable steel fibre–reinforced dry ultra-high performance concrete (DUHPC)." *J. Cleaner Prod.* 337 (Feb): 130507. https://doi.org/10.1016/j.jclepro.2022.130507.

Shen, D., J. Jiang, Y. Jiao, J. Shen, and G. Jiang. 2017. "Early-age tensile creep and cracking potential of concrete internally cured with pre-wetted lightweight aggregate." *Constr. Build. Mater.* 135 (Mar): 420–429. https://doi.org/10.1016/j.conbuildmat.2016.12.187.

Shen, D., J. Jiang, J. Shen, P. Yao, and G. Jiang. 2016. "Influence of curing temperature on autogenous shrinkage and cracking resistance of high-performance concrete at an early age." *Constr. Build. Mater.* 103 (Jan): 67–76. https://doi.org/10.1016/j.conbuildmat.2015.11.039.

Shen, D., J. Kang, Y. Jiao, M. Li, and C. Li. 2020. "Effects of different silica fume dosages on early-age behavior and cracking resistance of high strength concrete under restrained condition." *Constr. Build. Mater.* 263 (Dec): 120218. https://doi.org/10.1016/j.conbuildmat.2020.120218.

Shi, N., J. Ouyang, R. Zhang, and D. Huang. 2014. "Experimental study on early-age crack of mass concrete under the controlled temperature history." *Adv. Mater. Sci. Eng.* 2014 (Jan): 1–10. https://doi.org/10.1155/2014/671795.

Springenschmid, R., E. Gierlinger, and W. Kiernozicky. 1968. "Thermal stresses in mass concrete: A new testing method and he influence of different cements." In *Proc., 15th Int. Conf. on Large Dams (ICOLD)*, 57–72. Cham, Switzerland: Springer.

Viviani, M., B. Glisic, and I. Smith. 2007. "Separation of thermal and autogenous deformation at varying temperatures using optical fiber sensors." *Cem. Concr. Compos.* 29 (6): 435–447. https://doi.org/10.1016/j.cemconcomp.2007.01.005.

Vu, M.-H., J. Sulem, and J.-B. Laudet. 2012. "Effect of the curing temperature on the creep of a hardened cement paste." *Cem. Concr. Res.* 42 (9): 1233–1241. https://doi.org/10.1016/j.cemconres.2012.05.015.

Wang, Z., P. Sun, Y. Hu, and S. Han. 2023. "Crack morphology tailoring and permeability prediction of polyvinyl alcohol-steel hybrid fiber engineered cementitious composites." *J. Cleaner Prod.* 383 (Jan): 135335. https://doi.org/10.1016/j.jclepro.2022.135335.

Wei, Y., and W. Hansen. 2013. "Tensile creep behavior of concrete subject to constant restraint at very early ages." *J. Mater. Civ. Eng.* 25 (9): 1277–1284. https://doi.org/10.1061/(ASCE)MT.1943-5533.0000671.

Wei, Y., S. Liang, W. Guo, and W. Hansen. 2017. "Stress prediction in very early-age concrete subject to restraint under varying temperature histories." *Cem. Concr. Compos.* 83 (Oct): 45–56. https://doi.org/10.1016/j.cemconcomp.2017.07.006.

Yazici, S., G. Inan, and V. Tabak. 2007. "Effect of aspect ratio and volume fraction of steel fiber on the mechanical properties of SFRC." *Constr. Build. Mater.* 21 (6): 1250–1253. https://doi.org/10.1016/j.conbuildmat.2006.05.025.

Zhang, T., and W. Qin. 2006. "Tensile creep due to restraining stresses in high-strength concrete at early ages." *Cem. Concr. Res.* 36 (3): 584–591. https://doi.org/10.1016/j.cemconres.2005.11.017.

Zhao, Q., X. Liu, and J. Jiang. 2015. "Effect of curing temperature on creep behavior of fly ash concrete." *Constr. Build. Mater.* 96 (Oct): 326–333. https://doi.org/10.1016/j.conbuildmat.2015.08.030.

Zhao, Z., K. Wang, D. A. Lange, H. Zhou, W. Wang, and D. Zhu. 2019. "Creep and thermal cracking of ultra-high volume fly ash mass concrete at early age." *Cem. Concr. Compos.* 99 (May): 191–202. https://doi.org/10.1016/j.cemconcomp.2019.02.018.

Zheng, X., T. Ji, S. M. Easa, B. Zhang, and Z. Jiang. 2019. "Tensile basic creep behavior of lightweight aggregate concrete reinforced with steel fiber." *Constr. Build. Mater.* 200 (Mar): 356–367. https://doi.org/10.1016/j.conbuildmat.2018.12.138.